An analytic approach to the real-space transfer in semiconductor superlattices with highly doped barriers

1997 J. Phys.: Condens. Matter 9 7391

(http://iopscience.iop.org/0953-8984/9/35/013)

J. Phys.: Condens. Matter **9** (1997) 7391–7402. Printed in the UK PII: S0953-8984(97)81907-8

An analytic approach to the real-space transfer in semiconductor superlattices with highly doped barriers

V V Bryksin† and P Kleinert‡

† Physico-Technical Institute, Politekhnicheskaya 26, 194021 St Petersburg, Russia

‡ Paul-Drude-Institut für Festkörperelektronik, Hausvogteiplatz 5-7, 10117 Berlin, Germany

Received 17 February 1997

Abstract. The parallel transport in semiconductor superlattices and the associated transfer of electrons from high- to low-mobility layers are treated on the basis of quantum kinetic equations. Due to the assumed dominant role of impurity scattering in the barriers, the description of transport properties simplifies considerably. The superlattice band structure is replaced by a two-band model that simulates electronic states in the narrow quantum wells and in the adjacent broad barriers. Using the quasi-elastic approximation for the electron–phonon scattering in the narrow miniband, analytical results are derived for the current density that provide a qualitative understanding of the main physics taking place in the device. The approximate description of the real-space transfer encompasses scattering on acoustic and optical phonons as well as on impurities. Particular emphasis is put on the negative differential resistance and its dependence on the well width.

1. Introduction

Research into nonlocal nonlinear transport leading to N-shaped I–V characteristics with an associated static negative-differential-resistance (NDR) region has evolved considerably over the past decade [1]. One prominent example is the parallel transport in semiconductor superlattices composed of high-mobility wells spatially separated by low-mobility barriers. The transfer of electrons into the low-mobility region increases the resistance and may lead to NDR [1]. One transfer mechanism is due to tunnelling through potential barriers between adjacent wells. This so-called quantum-state transfer (QST) has been studied in [2–4]. Another mechanism is the real-space transfer (RST) where electrons are heated to energies higher than the barrier and transferred via thermionic emission [1]. In order to get an appreciable NDR effect due to the RST mechanism, the electronic properties must differ remarkably on different sides of the heterojunction. The possibility of obtaining an N-shaped NDR effect from the concept of RST has been demonstrated both experimentally and theoretically [1]. The experimental verification is difficult, because homogeneous fields are unstable in the NDR regime and the domain formation must be suppressed. A promising method is the fast-measuring technique that guarantees that the duration of the measurement is sufficiently short in comparison to the formation of domains. Such measurements were used to study nonlinear transport in bulk materials decades ago, and exploited by Masselink *et al* [5–7] to treat parallel transport in heterostructures. Furthermore, it has been demonstrated from a stability analysis of the homogeneous steady state that both homogeneous current oscillations and travelling field domains, associated with real-space transferred electrons, may exist [8–10].

0953-8984/97/357391+12$19.50

Although NDR effects can be confirmed experimentally, the study of their origin greatly benefits from theoretical investigations. This allows a physical understanding of the effects taking place in the device to be achieved and may be useful in optimizing the structure for a particular operation. Up to now most theoretical work in this field considered periodic structures and multiple quantum wells and relied on Monte Carlo simulations [11, 12] or electron temperature models [13, 14] (for a review see [1]). Although these calculations are designed to yield reliable numerical results and include, therefore, the interaction of electrons with phonons as well as the intervalley and alloy scattering, there remains the task of constructing a simple transparent theory with a minimum of assumptions and model parameters, in order to gain a deeper physical understanding of the main mechanisms. The states in the narrow high-mobility region of the RST structure are quantized, so quantum mechanical effects are strongly manifest. In this case the transport problem requires the consideration of quantum kinetic equations. The distribution functions of electrons that escape a localized state in quantum wells as an effect of a phonon-mediated real-space transfer have not been thoroughly investigated so far. The conventional Monte Carlo method does not apply to quantum transport, and quantum Monte Carlo calculations are still too time consuming to permit a realistic simulation.

Here we present a transparent quantum mechanical treatment of the hot-electron transport problem related to RST, which includes quantum wells separated by broad layers in which the quantization of the electron motion in the growth direction is not so essential. Our main objective in this paper is the development of an analytic theory that describes the spatial redistribution of electrons in superlattices due to accelerating parallel electric fields. In the next section the quantum kinetic equations are considered and solved analytically. In section 3 our basic results are used to derive an analytic expression for the current density, which describes RST of electrons between the low- and high-mobility transport channels under the influence of scattering on impurities as well as acoustic and optical phonons. Finally, section 4 summarizes our main results.

2. The quantum kinetic equations

The electronic transport in semiconductor superlattices is well described by the quantum kinetic equation for the Wigner transformed elements of the density matrix $f_\nu^{\nu'}(\boldsymbol{k})$, whose explicit spatial dependence leading to the domain formation is not taken into account. The elements of the density matrix with respect to the miniband indices ν and ν' are the solutions of the following integro-differential equation [15]:

$$\left\{\frac{e}{\hbar}\boldsymbol{E}\cdot\boldsymbol{\nabla}_{\boldsymbol{k}}+\frac{\mathrm{i}}{\hbar}[\varepsilon_{\nu'}(\boldsymbol{k})-\varepsilon_\nu(\boldsymbol{k})]\right\}f_\nu^{\nu'}(\boldsymbol{k})+\frac{\mathrm{i}e\boldsymbol{E}}{\hbar}\sum_\mu[\boldsymbol{Q}_{\mu\nu}(\boldsymbol{k})f_\mu^{\nu'}(\boldsymbol{k})-\boldsymbol{Q}_{\nu'\mu}(\boldsymbol{k})f_\nu^{\mu}(\boldsymbol{k})]$$
$$=\sum_{\mu\mu'}\sum_{\boldsymbol{k}_1}f_\mu^{\mu'}(\boldsymbol{k}_1)W_{\mu\nu}^{\mu'\nu'}(\boldsymbol{k}_1,\boldsymbol{k}) \tag{1}$$

where $\boldsymbol{E}$ is the constant electric field, $\varepsilon_\nu(\boldsymbol{k})$ the energy band structure of the νth miniband and $\boldsymbol{Q}_{\mu\nu}(\boldsymbol{k})$ the momentum matrix element:

$$\boldsymbol{Q}_{\mu\mu'}(\boldsymbol{k})=\frac{1}{\mathrm{i}}\sum_{\boldsymbol{G}}\chi_{\mu'}(\boldsymbol{k}+\boldsymbol{G})\,\boldsymbol{\nabla}_{\boldsymbol{k}}\chi_\mu^*(\boldsymbol{k}+\boldsymbol{G}). \tag{2}$$

$\boldsymbol{Q}_{\mu\nu}$ is a measure of the wavefunction overlap calculated from the superlattice envelope functions χ_μ ($\boldsymbol{G}$ is the reciprocal-lattice vector). The $\boldsymbol{Q}$-term in the kinetic equation (1) is associated with off-diagonal elements of the density matrix (f_2^1 and f_1^2 for a two-band

model) and describes electric-field-mediated transitions via Zener tunnelling. If the electric field is aligned parallel to the layers and nonparabolicity is not taken into account, this term vanishes because the corresponding component of the envelope function is simply given by the normalizing constant. Another transfer mechanism, which becomes relevant if the energy gap ε_g between two minibands is larger than the thermal energy of electrons $k_B T_e$ (with T_e being a characteristic electron temperature), is due to scattering on phonons or impurities described by off-diagonal elements of the scattering probability (W_{12}^{12} and W_{21}^{21} for a two-band model). In this paper we consider this special case and specialize to a two-band model. We retain besides the diagonal elements of the scattering probability only the interband matrix elements W_{12}^{12} and W_{21}^{21}. In this case the quantum kinetic equation (1) simplifies and takes the following form:

$$\frac{e}{\overline{h}}\boldsymbol{E}\cdot\boldsymbol{\nabla}_{\boldsymbol{k}} f_1^1(\boldsymbol{k}) = \sum_{\boldsymbol{k}'} f_1^1(\boldsymbol{k}') W_{11}^{11}(\boldsymbol{k}',\boldsymbol{k}) + \sum_{\boldsymbol{k}'} f_2^2(\boldsymbol{k}') W_{21}^{21}(\boldsymbol{k}',\boldsymbol{k}) \tag{3}$$

$$\frac{e}{\overline{h}}\boldsymbol{E}\cdot\boldsymbol{\nabla}_{\boldsymbol{k}} f_2^2(\boldsymbol{k}) = \sum_{\boldsymbol{k}'} f_2^2(\boldsymbol{k}') W_{22}^{22}(\boldsymbol{k}',\boldsymbol{k}) + \sum_{\boldsymbol{k}'} f_1^1(\boldsymbol{k}') W_{12}^{12}(\boldsymbol{k}',\boldsymbol{k}). \tag{4}$$

As we do not expect any significant effect due to Wannier–Stark localization, it is understood in equations (3) and (4) that the scattering probabilities do not depend on the electric field. Since only the diagonal elements of the distribution function enter equations (3) and (4) the notation can be simplified by dropping one band index ($f_\nu^\nu \to f_\nu$). Decomposing the distribution function into its symmetric and antisymmetric contributions the symmetric part of equations (3) and (4) can be written more explicitly as

$$\begin{aligned}\frac{e}{\overline{h}}\boldsymbol{E}\cdot\boldsymbol{\nabla}_{\boldsymbol{k}} f_\nu^a(\boldsymbol{k}) = {} & \sum_{\boldsymbol{q}} v_{\nu\boldsymbol{q}}^{ph}(\boldsymbol{k})\left\{ f_\nu^s(\boldsymbol{k}+\boldsymbol{q})\mathrm{e}^{(\varepsilon_\nu(\boldsymbol{k}+\boldsymbol{q})-\varepsilon_\nu(\boldsymbol{k}))/2k_BT} - f_\nu^s(\boldsymbol{k})\mathrm{e}^{-(\varepsilon_\nu(\boldsymbol{k}+\boldsymbol{q})-\varepsilon_\nu(\boldsymbol{k}))/2k_BT}\right\} \\ & + \sum_{\boldsymbol{q}} v_{12\boldsymbol{q}}^{ph}(\boldsymbol{k})\left\{ f_{\overline{\nu}}^s(\boldsymbol{k}+\boldsymbol{q})\mathrm{e}^{(\varepsilon_{\overline{\nu}}(\boldsymbol{k}+\boldsymbol{q})-\varepsilon_\nu(\boldsymbol{k}))/2k_BT} - f_\nu^s(\boldsymbol{k})\mathrm{e}^{-(\varepsilon_{\overline{\nu}}(\boldsymbol{k}+\boldsymbol{q})-\varepsilon_\nu(\boldsymbol{k}))/2k_BT}\right\} \\ & + \sum_{\boldsymbol{q}} v_{\nu\boldsymbol{q}}^{i}(\boldsymbol{k})\left\{ f_\nu^s(\boldsymbol{k}+\boldsymbol{q}) - f_\nu^s(\boldsymbol{k})\right\} + \sum_{\boldsymbol{q}} v_{12\boldsymbol{q}}^{i}(\boldsymbol{k})\left\{ f_{\overline{\nu}}^s(\boldsymbol{k}+\boldsymbol{q}) - f_\nu^s(\boldsymbol{k})\right\}\end{aligned} \tag{5}$$

where $\overline{\nu} = 2$ if $\nu = 1$ and vice versa. The electron–phonon matrix elements entering equation (5) are expressed by

$$\begin{aligned} v_{\nu\boldsymbol{q}}^{ph}(\boldsymbol{k}) = {} & 2\pi\overline{h}\frac{\omega_{\boldsymbol{q}}^2|\gamma_{\nu\nu}(\boldsymbol{q})|^2}{2\sinh(\overline{h}\omega_{\boldsymbol{q}}/2k_BT)}\Big\{\delta(\varepsilon_\nu(\boldsymbol{k}+\boldsymbol{q}) - \varepsilon_\nu(\boldsymbol{k}) - \overline{h}\omega_{\boldsymbol{q}}) \\ & + \delta(\varepsilon_\nu(\boldsymbol{k}+\boldsymbol{q}) - \varepsilon_\nu(\boldsymbol{k}) + \overline{h}\omega_{\boldsymbol{q}})\Big\}\end{aligned} \tag{6}$$

$$\begin{aligned} v_{12\boldsymbol{q}}^{ph}(\boldsymbol{k}) = {} & 2\pi\overline{h}\frac{\omega_{\boldsymbol{q}}^2|\gamma_{12}(\boldsymbol{q})|^2}{2\sinh(\overline{h}\omega_{\boldsymbol{q}}/2k_BT)}\Big\{\delta(\varepsilon_1(\boldsymbol{k}+\boldsymbol{q}) - \varepsilon_2(\boldsymbol{k}) + \overline{h}\omega_{\boldsymbol{q}}) \\ & + \delta(\varepsilon_1(\boldsymbol{k}+\boldsymbol{q}) - \varepsilon_2(\boldsymbol{k}) - \overline{h}\omega_{\boldsymbol{q}})\Big\}\end{aligned} \tag{7}$$

with $\gamma_{\nu\nu'}$ being the electron–phonon coupling constant and $\omega_{\boldsymbol{q}}$ the phonon frequency. Similar expressions hold for the elastic impurity scattering but their explicit form is not relevant for our present consideration.

Bearing in mind that an appreciable NDR effect only exists if the electronic properties differ remarkably in the two minibands, further progress in the analytic solution of equation (5) is related to studying such systems. The low-mobility carriers in the upper band will not

be heated significantly since the power input per electron is small. Therefore, it is a good first approximation to neglect electron heating in the upper band. In addition, it is reasonable to assume [4] that the impurity scattering is the most dominant interband scattering mechanism, too. Under these conditions the electron–phonon scattering contributions nearly compensate the small drift term on the left-hand side of equation (5), leading to considerable simplifications of the kinetic equation for electrons in the upper band. We obtain

$$\sum_{\boldsymbol{q}} v^i_{2\boldsymbol{q}}\delta(\varepsilon_2(\boldsymbol{k}+\boldsymbol{q})-\varepsilon_2(\boldsymbol{k}))[f^s_2(\boldsymbol{k}+\boldsymbol{q})-f^s_2(\boldsymbol{k})] + \sum_{\boldsymbol{q}} v^i_{12\boldsymbol{q}}\delta(\varepsilon_1(\boldsymbol{k}+\boldsymbol{q})-\varepsilon_2(\boldsymbol{k}))[f^s_1(\boldsymbol{k}+\boldsymbol{q})-f^s_2(\boldsymbol{k})]=0 \tag{8}$$

where the $\boldsymbol{k}$-dependence of the impurity matrix elements has been explicitly written down. Equation (8) expresses the fact that the particle balance under the influence of impurity scattering is essential for the determination of the symmetric part of f_2. This equation directly relates the distribution functions of the lower and upper bands, and has the simple solution

$$f^s_\nu(\boldsymbol{k}) = f(\varepsilon_\nu(\boldsymbol{k})) \tag{9}$$

where the up-to-now unknown function $f(\varepsilon)$ is determined from the remaining equation for the distribution function of the lower miniband ($\nu = 1$). As a result of this approximate treatment of electrons in the upper band, the distribution functions $f^s_\nu(\boldsymbol{k})$ depend on the band index ν and wavenumber $\boldsymbol{k}$ only via the energy dispersion relation $\varepsilon_\nu(\boldsymbol{k})$. On substituting the solution (9) into the kinetic equation (5) (for $\nu = 1$) the impurity contributions cancel each other and the distribution function is obtained from a kinetic equation that describes quasi-two-dimensional (Q2D) electrons in the narrow low miniband coupled to phonons. Consequently, equation (5) simplifies considerably and takes the following form for the narrow miniband ($\nu = 1$):

$$\frac{e}{\hbar}\boldsymbol{E}\cdot\boldsymbol{\nabla}_{\boldsymbol{k}} f^a_1(\boldsymbol{k}) = \sum_{\boldsymbol{k}'}[W(\boldsymbol{k}',\boldsymbol{k})f^s_1(\boldsymbol{k}')(1-f^s_1(\boldsymbol{k})) - W(\boldsymbol{k},\boldsymbol{k}')f^s_1(\boldsymbol{k})(1-f^s_1(\boldsymbol{k}'))]. \tag{10}$$

Within the momentum–time approximation the antisymmetric part is obtained from

$$f^a_\nu(\boldsymbol{k}) = -\frac{e\bar{h}}{m}\boldsymbol{k}\cdot\boldsymbol{E}\tau(\varepsilon_\nu(\boldsymbol{k}))\frac{\mathrm{d}f(\varepsilon_\nu(\boldsymbol{k}))}{\mathrm{d}\varepsilon_\nu(\boldsymbol{k})}. \tag{11}$$

For an energy-dependent scattering time τ, the unknown function $f(\varepsilon)$ is the solution of an integro-differential equation according to equations (9)–(11). The different current contributions in the lower and upper bands are calculated from $f^a_\nu(\boldsymbol{k})$. In equation (10) the scattering probability W accounts for electron–phonon scattering in a Q2D electron gas. Our consideration shows that the quantum mechanical description of NDR via the RST mechanism simplifies considerably due to the assumed large difference in the impurity scattering rate between the lower and upper minibands. The problem of solving the set of kinetic equations for the components of the distribution function reduces to the single-band case of an isolated Q2D electron gas. Within the framework of the quasi-elastic approximation, equations (10) and (11) are solved in the next section.

3. Solution of the kinetic equation in the quasi-elastic limit

In section 2 it has been demonstrated how the set of quantum kinetic equations simplifies for a RST structure exhibiting NDR. In this case the task of deriving an analytical solution for the distribution functions and the related current density becomes tractable. To proceed

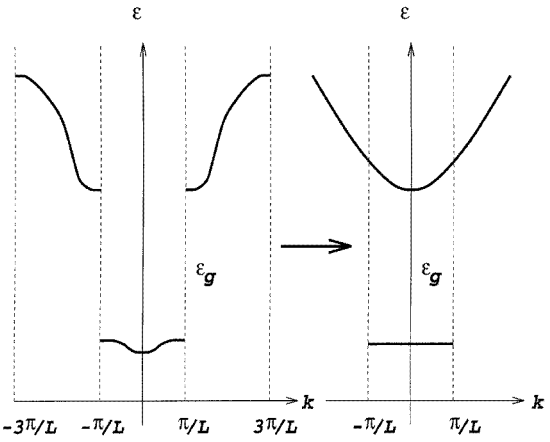

Figure 1. The superlattice energy band structure (left) and its approximate description in terms of quasi-2D and quasi-3D energy bands (right).

in this direction we replace the superlattice band structure by an energy dispersion that corresponds to a two-dimensional (2D) and three-dimensional (3D) electron gas related to the narrow miniband and broad upper superlattice bands, respectively. This replacement is illustrated in figure 1, where L denotes the superlattice period and ε_g the energy gap between the lowest miniband and the next one. Using these simplified dispersion relations we are able to derive a quantum mechanical description of how NDR may occur in a RST structure. This qualitative analysis is intended to emphasize the main physical mechanisms. To make further progress we will focus on the quasi-elastic scattering limit in the remaining part of the paper. In this case a momentum average of equations (10) and (11) results in an equation for the symmetric part of the distribution function f_1:

$$\begin{aligned}\frac{(eE)^2}{m} g_{2D}(\varepsilon)\varepsilon\tau(\varepsilon)\frac{\mathrm{d}f_1^s}{\mathrm{d}\varepsilon} &= \int_0^{\varepsilon} \mathrm{d}\varepsilon'\ g_{2D}(\varepsilon') \int_0^{\infty} \mathrm{d}\varepsilon''\ g_{2D}(\varepsilon'') \\ &\quad \times [W(\varepsilon', \varepsilon'') f_1^s(\varepsilon')(1 - f_1^s(\varepsilon'')) - W(\varepsilon'', \varepsilon') f_1^s(\varepsilon'')(1 - f_1^s(\varepsilon'))] \\ &\equiv \int_0^{\varepsilon} \mathrm{d}\varepsilon'\ I(\varepsilon') \end{aligned} \tag{12}$$

where $g_{2D}(\varepsilon) = \sum_{\boldsymbol{k}} \delta(\varepsilon - \varepsilon_1(\boldsymbol{k}))$ is the 2D density of states (DOS). The elastic part of the scattering probability is given by the momentum average

$$W(\varepsilon', \varepsilon) = \frac{1}{g_{2D}(\varepsilon) g_{2D}(\varepsilon')} \sum_{\boldsymbol{k},\boldsymbol{k}'} W(\boldsymbol{k}', \boldsymbol{k}) \delta(\varepsilon - \varepsilon_1(\boldsymbol{k})) \delta(\varepsilon' - \varepsilon_1(\boldsymbol{k}')). \tag{13}$$

As a next step within the framework of the quasi-elastic approximation, all terms in $I(\varepsilon)$ are expanded up to second order in $(\varepsilon - \varepsilon')$ [16]. Using this approximation we arrive at the representation

$$\begin{aligned} I(\varepsilon) = &-Q(\varepsilon) g_{2D}^2(\varepsilon) \left[\frac{f_1^s(\varepsilon)(1 - f_1^s(\varepsilon))}{k_B T} + \frac{\mathrm{d}f_1^s(\varepsilon)}{\mathrm{d}\varepsilon} \right] \\ &- \frac{D(\varepsilon)}{2} \frac{\mathrm{d}}{\mathrm{d}\varepsilon} \left(g_{2D}^2(\varepsilon) \left[\frac{f_1^s(\varepsilon)(1 - f_1^s(\varepsilon))}{k_B T} + \frac{\mathrm{d}f_1^s(\varepsilon)}{\mathrm{d}\varepsilon} \right] \right) \end{aligned} \tag{14}$$

which depends on the first energy moments

$$Q(\varepsilon) = \int_0^\infty \mathrm{d}\varepsilon' \ (\varepsilon' - \varepsilon) w(\varepsilon', \varepsilon) \qquad D(\varepsilon) = \int_0^\infty \mathrm{d}\varepsilon' \ (\varepsilon' - \varepsilon)^2 w(\varepsilon', \varepsilon). \tag{15}$$

The scattering probability $w(\varepsilon', \varepsilon) = W(\varepsilon', \varepsilon) \exp\left\{(\varepsilon - \varepsilon')/2k_BT\right\}$ is symmetric in ε and ε'. Making use of equation (14) and considering that $\mathrm{d}D(\varepsilon)/\mathrm{d}\varepsilon \approx 2Q(\varepsilon)$ is valid in the quasi-elastic limit, the following analytical solution is derived from equation (12):

$$f_1^s(\varepsilon) \equiv f(\varepsilon) = \frac{1}{A \exp y(\varepsilon) + 1} \tag{16}$$

which has the form of a Fermi distribution function with an electric-field-dependent exponent given by

$$y(\varepsilon) = \int_0^\varepsilon \frac{\mathrm{d}\varepsilon'}{k_B T_e(\varepsilon')} \qquad T_e(\varepsilon) = T[1 + 2(eE)^2 \varepsilon \tau(\varepsilon)/(m_1 D(\varepsilon) g_{2D}(\varepsilon))]. \tag{17}$$

T_e can be identified with an electric-field-dependent electron temperature. Starting from the kinetic equations we were able to demonstrate under which conditions the redistribution of carriers can be described by an effective-electron-temperature model. It is a peculiarity of equations (9), (16) and (17) that the electron temperatures of the two bands are expressed by the same function, but calculated at different energies. This simple result reminds of the paper by McCumber and Chynoweth [17] who treated intervalley transitions with a common electron temperature for different bands. The normalization constant A in equation (16) is determined from the electron density n via

$$n = \sum_{\boldsymbol{k}} (f_1^s(\boldsymbol{k}) + f_2^s(\boldsymbol{k})). \tag{18}$$

For a nondegenerate electron gas, Boltzmann statistics applies and A can explicitly be obtained from

$$A = n \Big/ \left[\frac{C_2}{L} \int_0^\infty \mathrm{d}\varepsilon \ \mathrm{e}^{-y(\varepsilon)} + C_3 \int_0^\infty \mathrm{d}\varepsilon \ \sqrt{\varepsilon} \mathrm{e}^{-y(\varepsilon + \varepsilon_g)} \right] \tag{19}$$

where constants have been introduced:

$$C_2 = \frac{m_1}{2\pi\hbar^2} \qquad C_3 = \frac{1}{(2\pi)^2} \left(\frac{2m_2}{\hbar^2} \right)^{3/2} \tag{20}$$

which are remnants of the 2D and 3D DOS, respectively. The current density is calculated from the antisymmetric part of the distribution functions (equation (11)) and the drift velocities according to

$$j = j_1 + j_2 \qquad j_i = e \sum_{\boldsymbol{k}} v_i(\boldsymbol{k}) f_i^a(\boldsymbol{k}). \tag{21}$$

From equations (11), (16), (19) and (21) our final analytical result for the current density is obtained:

$$j = \frac{e^2 E n}{m} \left(\frac{C_2}{L C_3} \int_0^\infty \mathrm{d}\varepsilon \ \mathrm{e}^{-y(\varepsilon)} \ \mathrm{d}(\varepsilon\tau(\varepsilon))/\mathrm{d}\varepsilon + \tau_{imp} \int_0^\infty \mathrm{d}\varepsilon \ \sqrt{\varepsilon} \mathrm{e}^{-y(\varepsilon + \varepsilon_g)} \right) \times \left(\frac{C_2}{L C_3} \int_0^\infty \mathrm{d}\varepsilon \ \mathrm{e}^{-y(\varepsilon)} + \int_0^\infty \mathrm{d}\varepsilon \ \sqrt{\varepsilon} \mathrm{e}^{-y(\varepsilon + \varepsilon_g)} \right)^{-1} \tag{22}$$

where τ_{imp} is the dominant scattering time of the upper 3D energy band that is due to impurity scattering. The quasi-two-dimensional electron gas has a high mobility, but a low DOS. The situation for the upper band is opposite. There the electrons have a low

mobility, but the DOS is high. At low electric fields, f_1^s approaches the Fermi function. In this case most electrons occupy the lowest miniband and the 3D current contribution is cut exponentially by the energy gap ε_g. Therefore, the current is mainly due to electrons that are accelerated in the high-mobility channels. With increasing electric fields, the electron temperature increases, so the exponential dependence on ε_g becomes ineffective. As the DOS of the 3D extended states exceeds the corresponding one of 2D electrons, the current starts to arise mainly from 3D electrons in the low-mobility barriers. We conclude that in the RST device considered, the asymptotic field dependence of the current is mainly determined by electrons in the high- (low-) mobility region of the sample at low (high) electric fields, which may give rise to NDR.

3.1. Scattering on acoustic phonons

In this subsection we will restrict our consideration to acoustic phonons, though at high electric fields the main cooling mechanism of electrons is due to emission of optical phonons. This artificial restriction is dropped in the next subsection but allows us here to derive simple results and to focus attention on the structure of our approach.

The scattering of electrons on acoustic phonons is well described within the quasi-elastic approximation. For a 2D electron gas the energy and momentum relaxation times have been determined in [18]. Using these results we obtain an expression for the electron temperature (17)

$$T_e = T\left(1 + \frac{4}{3}\frac{(eEl_0)^2}{W_0^2}\frac{m_1 s^2}{k_B T}\right) \tag{23}$$

which does not depend on the energy variable ε. In equation (23) the following energy and characteristic length scales have been introduced:

$$W_0 = \frac{\pi^2\hbar^2}{2m_1 L^2} \qquad l_0 = \frac{\pi\hbar^4\rho}{2m_1^3 E_1^2}. \tag{24}$$

Here s, ρ and E_1 are the sound velocity, material density and deformation potential constant, respectively. Inserting (23) into (17), the current density is easily calculated from equation (22) and we obtain

$$j = env_{ac}\left\{\frac{eEl_0}{k_B T}\frac{1 + (\tau_{imp}/\tau)Z(E)}{1 + Z(E)}\right\} \qquad Z(E) = \frac{\sqrt{\pi}}{2}\sqrt{\frac{k_B T_e}{W_0}}\mathrm{e}^{-\varepsilon_g/k_B T_e} \tag{25}$$

where the characteristic velocity $v_{ac} = 4m_1 Ls^2/3\pi\hbar$ has been introduced. The nonlinear field dependence enters the analytical expression (25) only through the electron temperature T_e.

Figure 2 shows the dimensionless current j/env_{ac} as a function of the electric field E for $\tau_{imp}/\tau = 0.01$, $T = 77$ K, $\varepsilon_g = 300$ meV and different layer widths. The upper dashed line is calculated with $L = 5$ nm and represents the current distribution j_1 which results from mobile electrons in the wells. The lower dashed line shows the second much smaller part j_2 of the current density resulting from electrons within the barriers. This large difference in the current densities lends further support to our approximate treatment of electrons in the barriers as nearly trapped (leading to equation (8)). Almost all of the curves exhibit weak N-shaped NDR characteristics. We remark that figure 2 does not show the additional linear L-dependence that enters the definition of the characteristic velocity v_{ac}. This leads to an increase of the low-field mobility with increasing well width, which is a consequence of the fact that the acoustic scattering time τ is proportional to L [19].

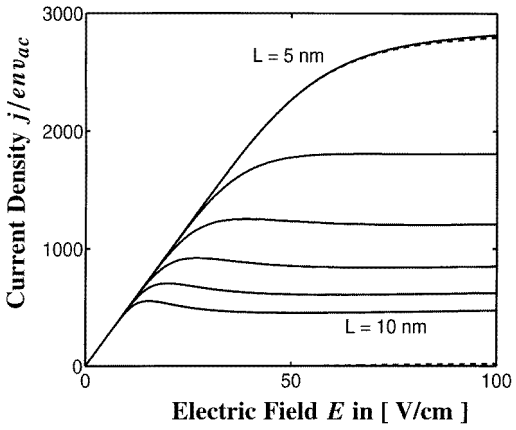

Figure 2. The current density j/env_{ac} as a function of the electric field for $T = 77$ K, $\varepsilon_g = 300$ meV, and $\tau_{imp}/\tau = 0.01$ as calculated from equation (25). From the top to the bottom solid curves the well width L was incremented in five steps from 5 nm to 10 nm. For comparison the dashed lines show the current contributions j_1 and j_2 (calculated with $L = 5$ nm) of electrons which reside in the wells and barriers, respectively.

For the large band-edge discontinuity between the minibands of adjacent layers that is considered ($\varepsilon_g = 300$ meV) the most important inelastic scattering process is due to optical phonons, so their influence cannot be neglected. Furthermore, a NDR effect at field strengths lower than 100 V cm^{-1} has never been observed in RST structures. That such an effect appears here is due to the unrealistic restriction to scattering on acoustic phonons. It is necessary to include scattering on optical phonons, which we will do in the next subsection.

3.2. Scattering on optical phonons

Now scattering on optical phonons is additionally taken into account. Here we will again restrict consideration to the quasi-elastic approach, and assume that the phonon subsystem is essentially undisturbed by the layered structure and closely resembles bulk phonons. The quasi-elastic approximation gives only a crude qualitative picture of optical phonon scattering in the 2D electron gas but nevertheless allows us here to provide a simple picture of the main physical mechanisms. The quasi-elastic contribution of the 2D scattering probability that comprises scattering-in and scattering-out rates due to the absorption and emission of polar optical phonons of energy $\hbar\omega_0$ is given by [20]

$$W(\varepsilon,\varepsilon') = \frac{L}{\hbar}\frac{|C|^2}{g_{2D}(\varepsilon)g_{2D}(\varepsilon')}\sum_{\boldsymbol{k},\boldsymbol{k}'}\delta(\varepsilon-\varepsilon(\boldsymbol{k}))\delta(\varepsilon'-\varepsilon(\boldsymbol{k}')) \times\{(N_0+1)I_{2D}(\boldsymbol{k}-\boldsymbol{k}')\delta(\varepsilon(\boldsymbol{k}')-\varepsilon(\boldsymbol{k})+\hbar\omega_0) + N_0 I_{2D}(\boldsymbol{k}'-\boldsymbol{k})\delta(\varepsilon(\boldsymbol{k}')-\varepsilon(\boldsymbol{k})-\hbar\omega_0)\} \tag{26}$$

where the coupling constant C of the Fröhlich Hamiltonian has been introduced:

$$C = \mathrm{i}\left[\frac{2\pi}{V}e^2\hbar\omega_0\left(\frac{1}{\varepsilon_\infty}-\frac{1}{\varepsilon_s}\right)\right]. \tag{27}$$

Here, V is the crystal volume, $N_0 = 1/(\exp(\hbar\omega_0/k_BT)-1)$ the phonon occupation number, and ε_∞ and ε_s are the optical and static dielectric constants, respectively. The Fourier

transformed Coulomb matrix element is expressed by [20]

$$I_{2D}(q_\parallel) = \frac{\pi}{2} L \left[\frac{1 - G(s)}{s^2} + \frac{1/2 + (2 - s^2/(s^2 + \pi^2))G(s)}{s^2 + \pi^2} \right] \tag{28}$$

where the following definitions have been used:

$$G(s) = \frac{1 - \mathrm{e}^{-2s}}{2s} \qquad s = \frac{q_\parallel L}{2}. \tag{29}$$

Performing the $\boldsymbol{k}$-, $\boldsymbol{k}'$-integrals in equation (26) we arrive at

$$w(\varepsilon, \varepsilon') = \frac{\delta(\varepsilon' - \varepsilon + \overline{h}\omega_0) S_e(\varepsilon) + \delta(\varepsilon' - \varepsilon + \overline{h}\omega_0) S_e(\varepsilon)}{2 g_{2D}(\varepsilon) \sinh(\overline{h}\omega_0 / 2k_B T)} \tag{30}$$

where the absorption and emission probabilities are expressed by

$$S_a(\varepsilon) = \frac{\alpha\omega_0}{\pi} \int_0^\pi \mathrm{d}\Phi \; \frac{k_0 I_{2D}(k_0)}{\sqrt{(\varepsilon/\overline{h}\omega_0)\cos^2\Phi + 1}} \tag{31}$$

$$S_e(\varepsilon) = \frac{\alpha\omega_0}{\pi} \int_0^{\Phi_m} \mathrm{d}\Phi \left[\left(\sum_{j=1,2} k_j I_{2D}(k_j) \right) \Big/ \sqrt{(\varepsilon/\overline{h}\omega_0)\cos^2\Phi - 1} \right] \Theta(\varepsilon - \overline{h}\omega_0) \tag{32}$$

with α being the Fröhlich coupling constant:

$$\alpha = \frac{e^2}{\overline{h}} \sqrt{\frac{m_1}{2\overline{h}\omega_0}} \left(\frac{1}{\varepsilon_\infty} - \frac{1}{\varepsilon_s} \right). \tag{33}$$

Depending on whether emission or absorption is considered, the energy and momentum conservation allows phonon wavevectors to have different values, determined by

$$\begin{aligned} k_0 &= k[-\cos\Phi + \sqrt{\cos^2\Phi + \overline{h}\omega_0/\varepsilon}] \\ k_j &= [\cos\Phi \pm \sqrt{\cos^2\Phi - \overline{h}\omega_0/\varepsilon}]. \end{aligned} \tag{34}$$

$\Phi_m = \arccos\sqrt{\overline{h}\omega_0/\varepsilon}$ is a cut-off relevant for phonon emission processes. From $1/\tau(\varepsilon) = \sum_{k'} W(k, k')$ and equation (30) one easily derives parameters that enter the exponent (equation (17)) of the distribution function. We obtain

$$\frac{1}{\tau(\varepsilon)} = \frac{\mathrm{e}^{-\overline{h}\omega_0/2k_BT} S_a(\varepsilon) + \mathrm{e}^{\overline{h}\omega_0/2k_BT} S_e(\varepsilon)}{2\sinh(\overline{h}\omega_0/2k_BT)} + 3\frac{s}{l_0} \frac{\sqrt{W_0} k_B T}{(2m_1 s^2)^{3/2}} \tag{35}$$

$$g_{2D}(\varepsilon) D(\varepsilon) = \frac{\overline{h}\omega_0}{2\sinh(\overline{h}\omega_0/2k_BT)} [S_a(\varepsilon) + S_e(\varepsilon)] + 2\varepsilon \frac{s}{l_0} \frac{W_0^{3/2}}{\sqrt{2m_1 s^2}} \tag{36}$$

where the first term on the right-hand side of these equations refers to scattering on polar optical phonons, whereas the second one comes from scattering on acoustic phonons. The current is calculated from equation (22) by considering equation (18) and inserting equations (35), (36) into equation (17). The final result for the current density provides a simple description of RST in multiple quantum wells subject to parallel electric fields. However, this approach is restricted to not-too-high field strengths. If the field exceeds a critical value the electrons gain more energy from the electric field than they lose by the polar optical phonon emission considered and the simulation does not converge. In this field region it is no longer possible to neglect heating processes of electrons in the barriers. In addition, such high-field excitations would result in an intervalley transfer, which is not accounted for by our present model.

Figure 3 shows numerically calculated current–field characteristics for different well widths L. In this calculation equal effective masses have been used for the accelerated

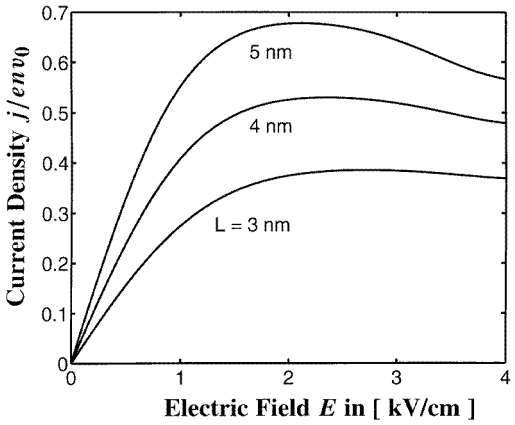

Figure 3. The field dependence of the current density for $T = 150$ K, $\varepsilon_g = 100$ meV, $\omega_0\tau_{imp} = 1$, and different layer widths L. Scattering on acoustic and polar optical phonons has been taken into account. v_0 is given by $v_0 = \hbar\omega_0\tau_{imp}/mL$.

motion of electrons in the lower and upper bands. In addition, the characteristic velocity $v_0 = \hbar\omega_0\tau_{imp}/mL$ has been introduced that depends on the layer width L, too. A current maximum appears in the field region between 2 and 3 kV cm^{-1}, which agrees with results of other more refined calculations and experiments [1]. With increasing layer widths the current maximum shifts to lower field strengths. The pronounced dependence of the current on the well width is a peculiarity of the RST mechanism that should be contrasted with intervalley transfer (the Gunn effect) giving rise to a current maximum at somewhat higher electric fields [1].

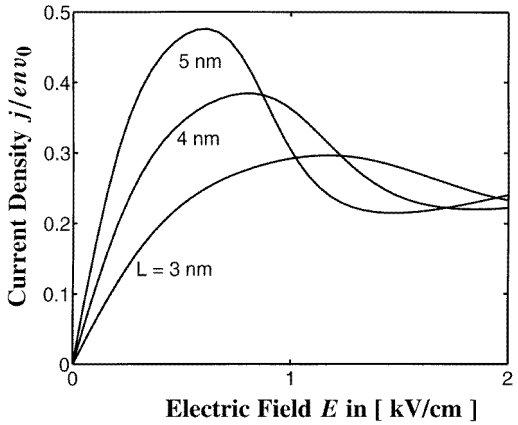

Figure 4. The field dependence of the current density as in figure 3 for scattering on acoustic and nonpolar optical phonons, with $D_1 = 1.1 \times 10^9$ eV cm^{-1}.

It is known that the energy dependence of both the scattering time and energy relaxation time in quasi-elastic scattering on polar and nonpolar optical phonons differs even qualitatively [21]. For scattering on polar optical phonons the 3D scattering time increases with increasing energy ε according to $\tau_{PO}(\varepsilon) \sim \sqrt{\varepsilon}$. On the other hand if the

scattering is due to nonpolar optical phonons the scattering time decreases with increasing ε ($\tau_{DO}(\varepsilon) \sim 1/\sqrt{\varepsilon}$). The transport properties turned out to be sensitive to these different asymptotic energy dependencies. Scattering on nonpolar optical phonons is easily treated within our approach by making use of the replacements $I_{2D} \to 1$ and

$$\frac{\alpha\omega_0}{\pi} \to \frac{3}{4\pi}\frac{D_1^2}{\omega_0 L^2 \rho}\frac{m_1}{\hbar^2}\sqrt{\frac{\hbar}{2m_1\omega_0}} \tag{37}$$

in equations (31) and (32). In equation (37), D_1 is the optical deformation potential constant. Figure 4 shows numerical results obtained for the same set of parameters as were used in figure 3.

Compared to the case for scattering on polar optical phonons, the current maximum shifts towards much lower fields and the current decrease in the NDR region is much more pronounced. Scattering on nonpolar optical phonons is relevant in Ge–Si-based multiple quantum wells, but is only of minor interest in GaAs–AlAs systems. The comparison between figures 3 and 4 reveals that the current–voltage characteristics sensitively depend on the particular scattering mechanisms that are used in the calculation.

4. Summary

Hot-electron thermionic emission due to electric fields parallel to the heterolayers has attracted a great deal of interest over the past decade. From a theoretical point of view RST diodes offer an attractive subject of research because there are still open problems to be addressed. Our objective was to consider quantum transport in a RST structure on the basis of a two-band model which accounts for quantum confinement in the well and the transfer into classical 3D regions in the barriers. An N-shaped I–V characteristic with a static NDR region is only observed when the impurity scattering dominates in the barriers with the result that there the electron heating effects are not very pronounced. In this case the set of kinetic equations considerably simplifies because heating in the upper band can be neglected, so only the particle balance plays a significant role. This approximation makes the derivation of an analytical solution feasible. Then the problem effectively reduces to the Boltzmann equation of a 2D electron gas subject to electron–phonon scattering. In order to grasp the main physics by avoiding extensive numerical calculations, we relied on the quasi-elastic approximation that is well justified for the treatment of scattering on acoustic phonons but yields only a qualitative picture of the scattering on optical phonons. A NDR effect is possible because electrons in the high-mobility wells acquire a high kinetic energy and are thermionically emitted into the barriers, where their mobility is much lower due to strongly enhanced impurity scattering, but where the DOS is larger than in the 2D well region. In contrast to the intervalley k-space transfer, which is not only observed in superlattice structures and multiple quantum wells but also in bulk materials, the RST effects strongly depend on the well width and the energy gap between the ground and first exited state. This peculiarity and the fact that the current maximum may appear at somewhat lower fields than in the related bulk material should allow the identification of NDR due to RST.

Our analytical approach was intended to focus on the main physics of the RST device. One step towards a theory that is even quantitatively reliable would be the numerical solution of the kinetic equations (10) and (11) for a 2D electron gas. There are also other possibilities for extending the treatment of RST presented. With obvious modifications the approach outlined in this paper can be used to investigate NDR observed in QST devices. In these structures the barriers are made sufficiently thin that tunnelling plays the dominant role. Such an approach could we hope cope with some open theoretical problems related to QST.

Acknowledgments

The authors thank M Asche for enlightening discussions. VVB acknowledges support by the Russian Foundation of Fundamental Research (Project No 96-02 16848-a)

References

[1] Gribnikov Z S, Hess K and Kosinovsky G A 1995 *J. Appl. Phys.* **77** 1337
[2] Pond J M, Kirchoefer S and Cukauskas E J 1985 *Appl. Phys. Lett.* **47** 1175
[3] Sawaki N, Suzuki M, Takagaki Y, Goto H, Akasaki I, Kano H, Tanaka Y and Hishimoto M 1986 *Superlatt. Microstruct.* **2** 281
[4] Jakumeit J, Tutt M and Pavlidis D 1994 *J. Appl. Phys.* **76** 7428
[5] Masselink W T, Braslau N, Wang W I and Wright S L 1987 *Appl. Phys. Lett.* **51** 1533
[6] Masselink W T, Braslau N, LaTulipe D, Wang W I and Wright S L 1988 *Solid-State Electron.* **31** 337
[7] Masselink W T 1989 *Semicond. Sci. Technol.* **4** 503
[8] Aoki K, Yamamoto K, Mugibayashi N and Schöll E 1989 *Solid-State Electron.* **32** 1149
[9] Schöll E and Aoki K 1991 *Appl. Phys. Lett.* **58** 1277
[10] Döttling R and Schöll E 1992 *Phys. Rev.* B **45** 1935
[11] Glisson T H, Hauser J R, Littlejohn M A, Hess K, Streetman B G and Shichijo H 1980 *Appl. Phys.* **51** 5445
[12] Gorfinkel V B, Kalfa A A, Solodkaya T I, Tager A S and Shofman S G 1986 *Fiz. Tekh. Poluprov.* **20** 881
[13] Shichijo H, Hess K and Streetman B G 1980 *Solid-State Electron.* **23** 817
[14] Garmatin A V and Kalfa A A 1985 *Fiz. Tekh. Poluprov.* **19** 2228
[15] Bryksin V V, Woloschin V C and Rajtzev A W 1980 *Fiz. Tverd. Tela* **22** 3076
[16] Yamashita J and Watanabe M 1954 *Progr. Theor. Phys. (Kyoto)* **12** 443
[17] McCumber D E and Chynoweth A G 1966 *IEEE Trans. Electron Devices* **13** 4
[18] Karpus V 1986 *Fiz. Tekh. Poluprov.* **20** 12
[19] Chattopadhyay D 1986 *Phys. Status Solidi* b **135** 409
[20] Leburton J P 1984 *J. Appl. Phys.* **56** 2850
[21] Gantmakher V F and Levinson Y B 1987 *Carrier Scattering in Metals and Semiconductors* (Amsterdam: North-Holland)